Dust in the diffuse ISM as revealed by DIRBE observations

J. P. Bernard, F. Boulanger, F. X. Désert, J. L. Puget, G. Helou, and W. Langer

Citation: AIP Conference Proceedings **348**, 105 (1996); doi: 10.1063/1.49251
View online: http://dx.doi.org/10.1063/1.49251
View Table of Contents:
http://scitation.aip.org/content/aip/proceeding/aipcp/348?ver=pdfcov
Published by the AIP Publishing

Dust in the diffuse ISM as revealed by DIRBE observations

J.P. Bernard, F. Boulanger, F.X. Désert, J.L. Puget
IAS, bât 121, Campus d'Orsay, 91405 Orsay Cedex, France.

G. Helou
IPAC/JPL, MS100-22, Pasadena CA, 91107, USA.

W. Langer
JPL, MS169-506, 4800 Oak Grove Drive CA, Pasadena CA 91109, USA.

ABSTRACT

The weekly averaged DIRBE full sky images have been processed to separate the various components contributing to the total brightness in the various bands. The zodiacal emission, which dominates at 12 and 25 μm and the zodiacal dust scattering at $\lambda < 5\,\mu$m are both accounted for using an empirical fit to the data. The diffuse stellar emission which dominates at $\lambda < 5\,\mu$m is determined using the shortest DIRBE photometric bands at 1.25 and 2.2 μm and a standard NIR extinction law. Preliminary results based on the first release of the DIRBE data have been presented in Bernard et al. 1994. When the zodiacal light and stellar emission are subtracted, significant emission remains above 2.2 μm, which follows the general distribution of the dust emission as seen in the IRAS bands. The DIRBE images therefore allow to extend our knowledge of the dust emission spectrum below 12 μm and above 100 μm. In the L(3.5 μm) and M(4.9 μm) bands, the dust emission can be seen not only toward the galactic plane but also in diffuse regions above the plane as well as toward closeby molecular complexes (ρ-Ophiuchi, Orion, Taurus,...). The existence of NIR dust emission in cold and diffuse regions strongly suggests transiently heated small dust particles as the carrier. The dust NIR spectrum is generally consistent with the dust model of Désert et al. 1990. In particular, the dust emission increases from 4.9 to 3.5 μm, which can be attributed to the contribution of the 3.3 μm emission feature of Polycyclic Aromatic Hydrocarbons (PAH). Significant continuum emission, or other feature emission, is also required to explain the observed brightness in the L band and the AROME ballon experiment results at low galactic latitude.

1. ZL subtraction

The thermal emission and scattering by dust associated to the solar system (Zodiacal Light: ZL) is visible in most all-sky DIRBE maps and often dominates the emission from the Galaxy. The thermal emission is particularily strong in the 12 and 25 μm bands but is also seen at 4.9 μm and above 60 μm, while at $\lambda \leq 5\,\mu$m, the ZL is dominated by scattered solar light. The ZL must therefore be precisely removed, in order to evidence weaker emission associated to the Galaxy.

In this study, we adopt an empirical approach to remove the ZL contribution from the DIRBE weekly averaged maps. Unlike more comprehensive methods based on physical models of the zodiacal cloud (see Reach et al. in this volume), this method arbitrarily removes any isotropic component present in the map. Therefore, the resulting subtracted maps cannot be directly used for the purpose of evidencing the cosmological IR background. However, it provides

maps with very little residus, which is very usefull in investigating the origin of the dust emission.

The data recorded by DIRBE during 1 week of observation cover about half the sky. Each weekly averaged map was binned into fixed intervals of solar elongation $E_\odot$ and the data in each bin, plotted as a function of eccliptic lattitude β, is fitted using the function proposed by Hauser 1993:

$$ZL(\beta) = A\,\beta_c/|\sin(\beta - \beta_0)|(1 - \exp(-\xi - \alpha\xi^2)) + B(\beta - \beta_0) \qquad (1)$$

$$\xi = |(\beta - \beta_0)/\beta_c|$$

where the amplitude A, the ecliptic latitude of the maximum β_0, the width β_c, the parameter α describing the behavior near $\beta = \beta_0$ and the slope of an additive baseline B are free parameters. In adjusting these parameters, the data points corresponding to the zodiacal bands at $\beta \simeq 9°$ and/or affected by strong galactic emission are ignored. At a given solar elongation, the fit is peformed independently into 2 zones of ecliptic longitude and for $\beta \leq \beta_0$ and $\beta \geq \beta_0$, leading to 4 sets of parameter values for each solar elongation bin and week. The accuracy of the fit is generally better than a few percent of the ZL intensity at $12\,\mu$m for one profile.

The above procedure is repeated for each of the 41 weekly averaged maps and the fitted values for each free parameter are gathered into 4 maps on a regular grid of week number and solar elongation. The individual parameters show systematic variations in these coordinates, which reflect properties of the zodiacal cloud as seen from varying location along the earth orbit. The amplitude A decreases with angular distance from the sun roughly as $1/E_\odot$. The peak position β_0 varies with time as a 1 year period sin function, due to the inclination of the zodiacal cloud on the ecliptic plane. The width β_c steadily increases toward high solar elongation, probably reflecting actual radial variations of the shape of the zodiacal cloud with distance from the sun (see Reach et al.). Each parameter map is then fitted using a smooth 2D function matching the behavior described above, or a low order polynomial if no systematic trend is observed. The smooth parameter surfaces are then interpolated to construct the ZL estimate for each pixel of each weekly average map, using equation 1. After subtraction of the ZL, all 41 week maps are averaged into an annual average map. As ZL subtraction absolute uncertainties are smaller at high solar elongation, we restricted the annual average to $E_\odot \geq 90°$ and used a weighting fuction proportional to $1/E_\odot$. The procedure was repeated independently for all DIRBE bands from 1.25 to $100\,\mu$m, leading to a set of subtracted annual maps. Due to the weakness of the ZL contribution at $\lambda > 100\,\mu$m, the above procedure cannot be applied and unsubtracted maps were used in the following at 140 and $240\,\mu$m.

2. Stellar light subtraction

The stellar light from the Galaxy dominates the total sky brightness below $\lambda = 5\,\mu$m in the DIRBE data. It includes emission from individual bright stars, as well as a diffuse stellar component produced by late type stars. This emission as to be removed, in order to evidence dust emission below $5\,\mu$m.

The subtraction of the diffuse component can be done efficiently assuming that (1) the sky brightness in the DIRBE 1.25 and $2.2\,\mu$m bands is dominated by star light (i.e. the dust emission in these bands can be neglected relative to the

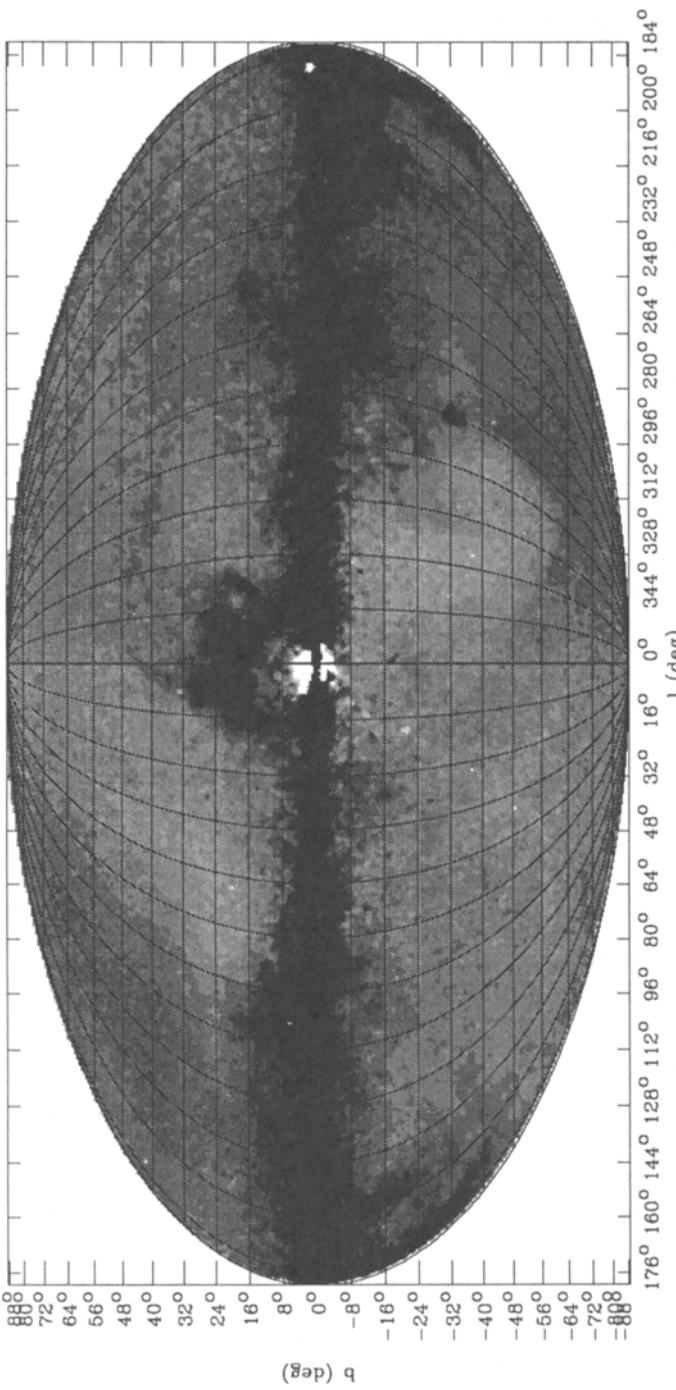

Fig 1: Dust emission in the L(3.5 μm) DIRBE band.

stellar emission) and (2) the dust clouds are mainly located in front of most of the stellar diffuse emission. The last assumption is generally verified along line of sights above a few degrees above the plane because the scale height of dust is smaller than that of stars. It may however fail toward the plane. Under these assumptions, the intrinsic stellar colors are related to the observed intensities through

$$(I^*_\lambda/I^*_{1.25})_{\rm int} = I^*_\lambda e^{\tau_\lambda}/I^*_{1.25}e^{\tau_{1.25}}. \quad (2)$$

The diffuse stellar contribution in any DIRBE band therefore writes

$$I^*_\lambda = I^*_{1.25}\,(I^*_\lambda/I^*_{1.25})_{int}\,e^{(-a_\lambda \tau_{1.25})}$$

where $a_\lambda = \tau_\lambda/\tau_{1.25}$ is taken from the average IR extinction law derived by Rieke and Lebofsky 1985. $\tau_{1.25}$ can be derived from eq 2:

$$\tau_{1.25} = (a_{2.2} - 1)^{-1} \ln[I^*_{1.25}/I^*_{2.2}(I^*_{2.2}/I^*_{1.25})_{\rm int}]$$

The intrinsic colors are derived by averaging into the DIRBE maps in regions of low dust emission and low $\tau_{1.25}$. The colors derived ($(I^*_{1.25}/I^*_{2.2})_{int} = 1.4$, $(I^*_{1.25}/I^*_{3.5})_{int} = 2.8$, $(I^*_{1.25}/I^*_{3.5})_{int} = 6$) are in general agreement with those measured by Arendt et al. 1994 extrapolated to low extinction. The diffuse stellar contribution derived above was subtracted from DIRBE maps in the L(3.5) and M(4.9) bands and the remaining contribution from individual stars was subtracted using a simple median filter. At IRAS wavelengths, the IRAS PSC convolved to the DIRBE beam pattern was used to subtract the contribution of known IRAS point sources. The dust map obtained in the L band after subtraction of the ZL and stellar emission is shown in figure 1. Low frequency residuals of the ZL subtraction can be seen near the ecliptic poles. Toward the Galactic center, the stellar diffuse emission is over subtracted because of the peculiar intrinsic colors of the stars in the bulge.

3. Discussion

The maps subtracted from ZL and stellar emission show extended emission down to the L band. The spatial distribution correlates closely to the dust thermal emission at $\lambda > 100\,\mu$m and the observed brightness levels are 1 to 2 order of magnitude above what is expected from stellar scattered light at the surface of clouds (Cutri, private comunication). We therefore attribute the L and M emission to dust emission. Figure 1 shows that the L band emission is mainly located along the galactic plane ($|b| < 10°$) and in well known high latitude regions such as ρ-ophiuchi ($-20° < l < 20°$, $10° < b < 32°$), Taurus ($155° < l < 180°$, $-20° < b < -10°$), Orion ($200° < l < 220°$, $-20° < b < -10°$), ... The short wavelength emission can often be followed up to $|b| \simeq 40°$. A similar behavior is observed in the M band, although stronger residuals of the ZL subtraction are present in the map and the dust emission is generally weaker.

3.1 *Comparison with the AROME data*

Along the Galactic plane, the emission in the $3.3\,\mu$m PAH feature and the adjacent continuum has been observed by the AROME balloon born experiment (see Giard et al. 1994). The agreement between the AROME data and

the DIRBE total L band emission map was found to be $\simeq 5\%$, well within the calibration uncertainty of the AROME data (see Bernard et al. 1994). The comparison also reveals that the prominent regions emitting the 3.3 μm feature along the Galactic plane are also maxima of the L DIRBE map in figure 1. However, the 3.3 μm feature detected by AROME contributes to only about 20% of the DIRBE L band dust emission. This ratio seems constant with Galactic latitude in the range $-50° < l < 30°$. This indicates that the regions emitting the PAH feature along the galactic plane also contribute to a strong 3 μm continuum. It is worth noticing that, in order to explain both the L and M DIRBE dust emission with 20% of the L band produced by the feature, the underlying continuum should have colors comparable to the continuum observed by Sellgren et al. 1990 toward reflection nebulae ($T \simeq 800\,K$). Wether or not the continuum is also present at high galactic latitude cannot be answered with the present data only, as no 3.3 μm feature observation of high or intermediate latitude cirrus clouds is yet available. Note that significant continuum dust emission at high latitude could seriously affect the transparency of the cosmological window near 3 μm. The IRTS and ISO satellites will soon bring data relevant to this important issue.

3.2 *Average colors and comparison to the PAH dust model*

In order to derive average colors for the dust emission, the DIRBE maps described above were averaged for various individual clouds. The template for clouds ($\tilde{I}_{100}$) is the full sky 100 μm DIRBE map filtered using a lowest percentile filter in elongated boxes of galactic longitude in order to remove low spatial frequency variations along galactic latitude. Individual clouds are defined as contiguous regions above a given threshold (Thr) in $\tilde{I}_{100}$. We then define a background region (1.2° wide with $\tilde{I}_{100} < Thr$) surrounding each cloud. At each wavelength, a low degree polynomial surface is fitted in the background region, in order to subtract any remaining background and the data in the cloud region with $Thr < \tilde{I}_{100} < Thr + \Delta Thr$ is used to produce the average spectrum. The threshold is then increased by ΔThr and the above steps are repeated. This procedure allows to separate the often closely associated diffuse extended regions from the bright localized ones (e.g. HII regions) that can easily dominate the total emission of a given cloud, without counting any individual region twice. The average spectra of individual regions with various average 100 μm brightness are shown in fig 2, normalized to 240 μm. The spectra with high average 100 μm brightness ($\overline{I}_{100}$) correspond to hot and bright clouds, generally located close to the galactic plane. It can be seen that the lowest spectra, corresponding to the most diffuse regions, agree well with the PAH model by Désert et al. 1990. Going from low to high $\overline{I}_{100}$, the NIR and IR spectrum increases as a whole, so that bright clouds generally have higher NIR/FIR ratio. Such a behavior is expected under the PAH model if hot clouds are illuminated by higher energy UV photons (e.g. due to the presence of closeby young stars) which are preferentially absorbed by small particles, or if hot clouds have higher small particles abundances. Note that a relative decrease of the 12 μm emission is generally observed in the IRAS data around highly irradiated regions such as HII regions (e.g. Ryter et al. 1987), which is attributed to the destruction of the smallest particles in high UV density regions. This trend is also observed in the average colors at $\overline{I}_{100} > 100$ MJy/sr (not shown in figure 2). The NIR

increase with $\overline{I}_{100}$ is specially strong at wavelengths corresponding to continuum in the dust model (e.g. 4.9, 25, 60 μm) and only moderate in the PAH feature dominated bands (3.5 and 12 μm). This trend will have to be explored in more details using the model, and may require a larger feature/continuum ratio of the PAH emission, in particular in the 10 μm region.

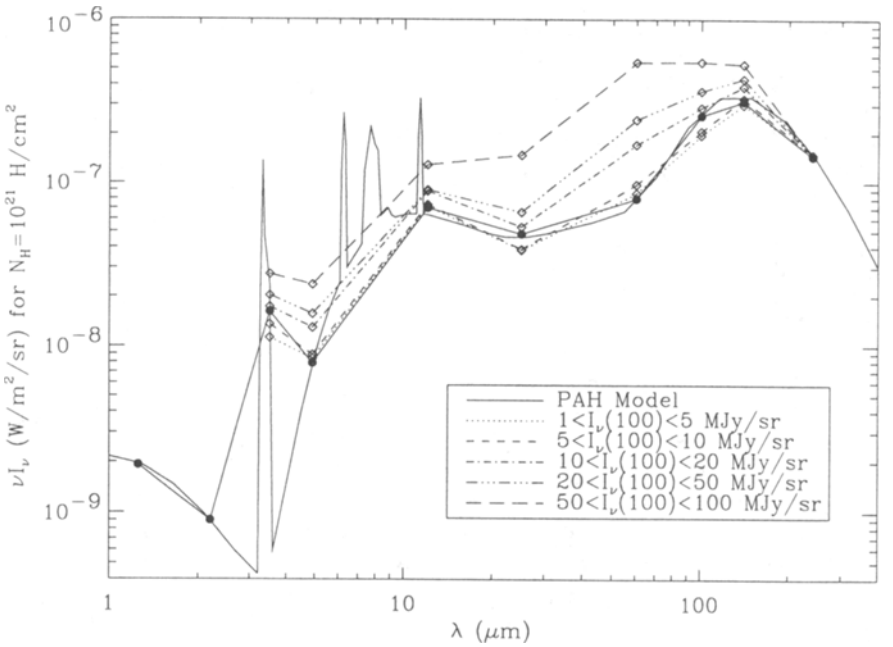

Fig 2: Prediction of the PAH model (dots) and DIRBE average colors.

4. Conclusions

The zodiacal light and stellar emission has been subtracted from the DIRBE all-sky maps from 3.5 to 100 μm, in order to evidence galactic dust emission. Significant emission is found down to the 3.5 μm DIRBE band and up to galactic latitudes as high as 40°. The spatial distribution of the DIRBE M(4.9 μm) and L(3.5 μm) band emission are generally very similar. The NIR emission follows the IR and FIR distribution and cannot be attributed to starlight scattering at the clouds surface but must be interpreted as dust emission. Average dust emission spectra of individual regions over a range of excitation conditions has been built. The spectral energy distribution of low brightness, high latitude regions is in good agreement with the predictions of the PAH model in the solar neighborhood. The average NIR/FIR ratio increases with increasing excitation, which also seems in qualitative agreement with the model, although a more detailed analysis is required. The spatial distribution of the L and M dust emission closely follows the 3.3 μm PAH feature emission observed by the AROME experiment along the galactic plane, but a strong NIR continuum ac-

counting for as much as 80% of the DIRBE L band dust emission is also required to explain the DIRBE L band emission levels at low latitude.

Acknowledgements

We are grateful to the Goddard Space Flight center team for their help in reducing the DIRBE data. This work was conducted in part at the Jet Propulsion Laboratory, California Institute of Technology under contract to NASA and supported in part under the LTSA program and a post-doctoral fellowship from the European Space Agency.

References

Arendt R.G. et al., 1994 ApJ Let 425, 85.
Bernard J.P., Boulanger F., Puget J.L. 1993, A&A 277, 609.
Bernard J.P., Boulanger F., Désert F.X., Giard M., Helou G., Puget J.L., 1994, A&A Let 291, L5.
Désert F.X., Boulanger F., Puget J.L., 1990, A&A 273, 215.
Giard M. et al. 1994, A&A 286, 203.
Hauser M.G. 1993 in AIP Conf. Proc. 278, "Back to the Galaxy", eds S.S. Holt, F. Verter.
Rieke G.H., Lebofsky M.J., 1985, ApJ 288, 618.
Ryter C., Puget J.L., Pérault M., 1987, A&A 186, 312.
Sellgren K., Tokunaga A.T., Nakada Y., 1990, ApJ 349, 120.